Impact of Alloy-Disorder-Induced Localization on Hole Diffusion in Highly Excited *c*-Plane and *m*-Plane (In,Ga)N Quantum Wells

Ramūnas Aleksiejūnas,[1] Kazimieras Nomeika,[1,*] Oleg Kravcov,[1] Saulius Nargelas,[1] Leah Kuritzky,[2] Cheyenne Lynsky,[2] Shuji Nakamura,[2] Claude Weisbuch,[2,3] and James S. Speck[2]

[1] *Institute of Photonics and Nanotechnology, Vilnius University, Saulėtekio Avenue 3, Vilnius LT-10257, Lithuania*

[2] *Materials Department, University of California, Santa Barbara, California 93106, USA*

[3] *Laboratoire de Physique de la Matière Condensée, Ecole Polytechnique, CNRS, IP Paris, Palaiseau Cedex 91128, France*

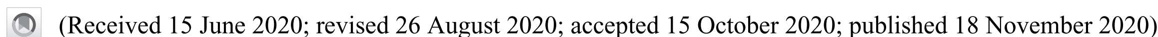

(Received 15 June 2020; revised 26 August 2020; accepted 15 October 2020; published 18 November 2020)

The diffusion coefficient of holes can provide knowledge about carrier localization in (In,Ga)N, where the carrier dynamics are altered by randomly fluctuating potential landscape. In group-III nitrides, the diffusivity of holes is difficult to measure by electrical methods but it can be studied using optical techniques. Here, we investigate the dependence of the hole diffusion coefficient on direction and carrier density in *c*-plane and *m*-plane (In,Ga)N structures by employing the light-induced transient-grating technique. We show that the hole diffusion coefficient is anisotropic in the *m*-plane structure, where it is several times larger along the *a* crystallographic direction than along the *c* direction. Such anisotropy is observed within the broad range of carrier densities from 10^{18} to 10^{20} cm^{-3}. The diffusivity changes nonmonotonously with increasing photoexcitation, this dependence being different in thick and thin layers. We argue that an unexpectedly high diffusion coefficient at low carrier densities in thick quantum wells can be a signature of efficient hole transport via percolative paths occurring due to compositional disorder. In turn, a decrease of diffusivity with the excitation can reflect the effect of Coulomb blockade of these paths. Finally, we demonstrate that disorder impacts carrier diffusivity even at carrier densities above 10^{19} cm^{-3}, where the overflow of localized states must be included to explain the observed increase of the diffusion coefficient with the carrier density.

DOI: 10.1103/PhysRevApplied.14.054043

I. INTRODUCTION

The ternary nitride alloys (In,Ga)N and (Al,Ga)N are currently the materials of choice for light-emitting diodes (LEDs) operating in the visible and ultraviolet spectral range. A key requirement for any LED material is to have a high internal quantum efficiency (IQE), which is an internal material property defined as the ratio of the radiative to the overall recombination rates. Surprisingly, the (In,Ga)N compound is capable of IQE values above 90% despite the extremely high threading dislocation densities, which typically exceed $10^7 - 10^8$ cm^{-2} [1,2]. Cathodoluminescence (CL) data have confirmed that threading dislocations indeed act as the nonradiative recombination centers in (In,Ga)N [3,4]. It has been proposed that localization of charge carriers may be the process that hinders carrier transport and, thus, limits nonradiative recombination at dislocations [5].

The presence of carrier localization in (In,Ga)N structures has been demonstrated both experimentally and theoretically. Localization occurring on a very small scale of 5 nm has been observed directly using scanning tunneling luminescence [6]. Strong hole and weaker electron localization have been proven in several studies, where photoluminescence (PL) and CL measurements have been combined with atomistic calculations [7–12]. Carrier localization is expected to have broad implications that are still being studied and discussed, e.g., a possible link with the "green-gap" problem [13,14], local modification of the recombination constants [15], whether the release of carriers with increasing excitation can contribute to the efficiency droop [16,17], etc.

Solutions to the above-mentioned problems would benefit from better knowledge of localization parameters that, unfortunately, are difficult to measure. Most often, the only known localization parameter is the spectral distribution of the localized states deduced from the "S shape" of the PL peak temperature dependence [18]. On the other hand, it is reasonable to assume for inorganic semiconductors that carriers in the localized states are immobile and that carrier transport occurs via the extended states [19]. Therefore, the transport coefficients must reflect the contribution of

*kazimieras.nomeika@ff.vu.lt

 © 2020 American Physical Society

localization when a considerable fraction of the nonequilibrium carriers become trapped in the abundant and deep localized states. In particular, it has been shown that the localization–thermal-release cycle alters the diffusion coefficient of charge carriers [19,20]. Since the holes are strongly localized in (In,Ga)N [8], the hole diffusivity can be a valuable source of information about the localization conditions in a sample. This idea can also be applied beyond nitrides: it has been demonstrated that carrier diffusion in GaAs depends on excitation due to hole trapping by defect states that can be saturated by increasing the carrier density [21,22]. Electrical methods such as Hall measurements rely on the Einstein relation to yield the diffusion coefficient but its applicability is uncertain for highly disordered systems [23,24]. Another option is to use optical methods that measure the ambipolar diffusion coefficient, which, under band-to-band excitation, is governed by hole transport [25].

The ambipolar diffusion coefficient in (In,Ga)N is usually measured using scanning near-field optical microscopy (SNOM) [26], time-of-flight [27], or light-induced transient-grating (LITG) techniques [28]. The former are based on determination of the carrier diffusion length L_D and calculation of the diffusivity D if the carrier lifetime τ is known: $L_D^2 = D\tau$. This approach has been used in several publications to determine the diffusion coefficient in polar (In,Ga)N quantum wells (QWs) [27,29–31]. Also, a modified multimode SNOM setup has been applied to measure the diffusivity in a nonpolar (In,Ga)N QW sample [32]. While allowing for high spatial resolution, the time-of-flight and SNOM-based measurements also have several limitations, such as diffusivity determination from the lifetime-dependent diffusion length and difficult calibration of the photoexcitation. The LITG technique, in contrast, provides a spatially integrated approach and also allows for more accurate calibration of the photoexcited carrier density. The ability of LITG to access very high carrier densities allows studies that are relevant for the IQE droop regime. Furthermore, the technique provides a rather direct measurement of D by separately determining the carrier lifetime and diffusion length. The LITG technique has been used in several publications to study the diffusion coefficient and its dependence on the carrier density and temperature [17,33–35], the authors having concluded that carrier localization indeed affects the ambipolar diffusion coefficient D. However, these studies have also left many unanswered questions, including the possible role of the built-in electrical field or other high-density effects that can influence the diffusivity, such as band degeneracy or electron-hole scattering.

To address these less-investigated aspects of carrier transport in (In,Ga)N quantum structures, we apply the LITG technique to investigate intrawell carrier transport and its dependence on the carrier density and diffusion direction with respect to the crystallographic axes in polar and nonpolar (In,Ga)N QW structures. To better understand the possible impact of various high-density processes on the value of the ambipolar diffusion coefficient D, we fit the obtained data to a model, which accounts for the carrier localization, degeneracy, and electron-hole scattering. As a result, we are able to confirm that the ambipolar diffusion coefficient is a measure of the hole diffusivity, which is very anisotropic in m-plane samples, and that the hole diffusion is strongly affected by carrier localization even at carrier densities above 10^{18} cm^{-3}. We also show that the dependence of the diffusion coefficient on the carrier density in thick nonpolar QWs is not typical for (In,Ga)N QW structures and we present possible explanations. Finally, we discuss the relevance of the obtained results to LED applications.

II. EXPERIMENT

In this work, we use four different (In,Ga)N structures, all grown by metalorganic chemical vapor deposition. Two samples are deposited on c-plane sapphire substrate, followed by a 3-μm-thick unintentionally doped GaN buffer layer. Onto such a template, we deposit either ten pairs of 3-nm-thick $In_{0.1}Ga_{0.9}N$ QWs–10 nm GaN barriers in the "c-MQW" sample or a 58-nm-thick $In_{0.1}Ga_{0.9}N$ single layer in the "thick-c-layer" sample. Both structures are protected by an 8-nm-thick GaN cap layer. The other two m-plane structures have identical structures, except for the QW thickness. They are grown on an m-plane GaN substrate miscut by -1° toward the [0001] direction. On the substrate, a homoepitaxialy grown approximately 1.2-μm-thick Si-doped GaN buffer layer is followed by three periods of either 8-nm- ("thick m-plane MQW") or 4-nm-thick ("thin m-plane MQW") $In_{0.13}Ga_{0.87}N$ QWs, separated by 9-nm-thick barriers. On top, a 7.5-nm $Al_{0.22}Ga_{0.78}N$ electron blocking layer and a 143-nm p-doped GaN cap layer are deposited.

We employ the LITG technique to measure the ambipolar diffusion coefficient, D_a, and the carrier lifetime, τ, in different directions and at various excitation levels. In the LITG experiment, an interference pattern of two laser beams is used to create a spatially periodic distribution of nonequilibrium carriers in a sample [28]. Figure 1(a) illustrates the basic LITG setup used for this study. The experiment is based on the PHAROS (Light Conversion) laser, which emits 250-fs-duration pulses at a 1030 nm fundamental wavelength at a 30 kHz repetition rate. The laser beam is divided into pump and probe parts. The pump wavelength is tuned to 394 nm using an ORPHEUS (Light Conversion) optical parametric amplifier. The pump wavelength is chosen to photoexcite only the (In,Ga)N QWs but not the GaN layers. To achieve spatially periodic excitation of the sample, we use a holographic beam splitter (HBS) to divide the pump beam into two equal parts (the

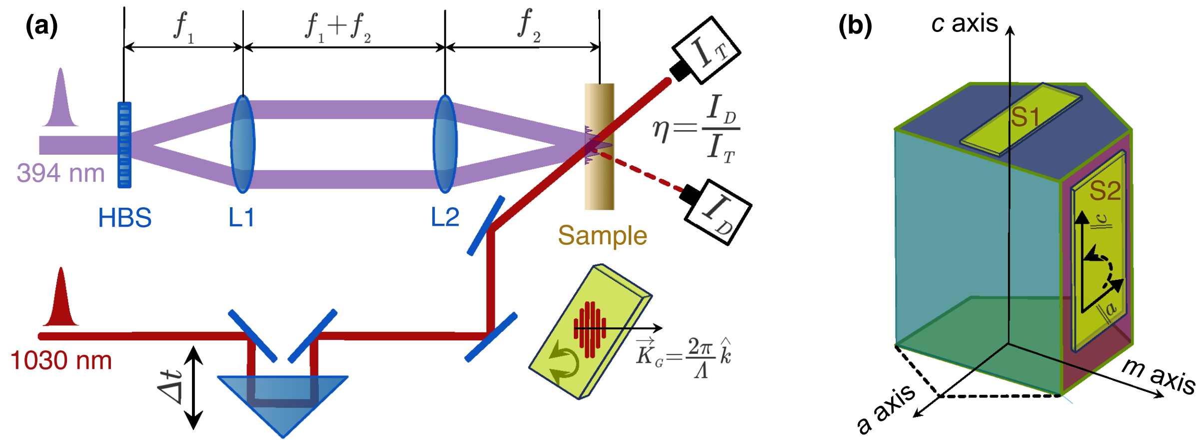

FIG. 1. (a) The light-induced transient-grating (LITG) experimental setup. (b) The orientation of the samples with respect to the crystallographic axes.

beams diffracted into ±1 orders are used), which are later combined by the lenses L1 and L2 and interfered on the sample surface [36]. The periodic light field photoexcites the nonequilibrium carrier pattern that repeats the periodicity of the photoexcitation, thus recording a transient diffraction grating. The direction of the carrier density gradient is parallel to the transient-grating vector K_g, while the grating period Λ can be varied by using one of the several beam splitters with different periods. We use HBSs with periods of 10, 11.7, 16, and 40 μm, which results in transient diffraction gratings on the sample with periods of $\Lambda = 2.47$, 2.91, 4.0, and 9.93 μm, respectively. The exact period of the transient gratings is measured from the phase shift of the diffracted signal [37]. The direction of carrier diffusion with respect to the sample crystallographic orientation is changed by rotating the sample as illustrated in Fig. 1 (b). The photoexcited carrier density N_0 is varied by changing the energy flux ("excitation") of the pump pulse. At the end of the pulse, N_0 can be estimated as $N_0 = (1 - R)\alpha I_0/h\nu$, where $R = 0.21$ is the the reflection coefficient, $\alpha = 1.3 \times 10^5$ cm^{-1} is the (In,Ga)N absorption coefficient at the pump wavelength [34], I_0 is the pump pulse intensity, and $h\nu$ is the pump photon energy. We estimate the photogenerated carrier density by measuring the light absorption in an integrating sphere and find good agreement (within 10%) with the N_0 expression above. The 394-nm excitation wavelength has sufficiently high energy relative to the absorption edge (the band gap) in the (In,Ga)N QWs to avoid absorption bleaching due to the Burstein shift [38] at the lower energies in the QWs [39].

The transient grating is probed by monitoring the diffraction of a probe pulse at 1030 nm, which is arbitrarily delayed with respect to the pump pulse. The diffraction is quantified by the diffraction efficiency η, which is defined as the ratio between the intensities of the diffracted I_D and transmitted I_T parts of the probe beam. Using the classical Drude theory, $\eta(t)$ can be expressed in the following form [28]:

$$\eta(t) = \left(\frac{\pi\, d n_{\mathrm{eh}} N(t)}{\lambda}\right)^2 = \left(\frac{\pi\, d n_{\mathrm{eh}} N_0}{\lambda}\right)^2 \exp\left(-\frac{2t}{\tau_G}\right), \tag{1}$$

where d is the thickness of the photoexcited material, n_{eh} is the refractive index change due to a single electron-hole pair, $N(t)$ is the density of carriers at time t, N_0 is the density of photoexcited carriers at the end of the pump pulse, λ is the wavelength of the probe beam, and τ_G is the time constant of the transient-grating decay.

For light frequencies far from resonance, n_{eh} is equivalent to the following [28]:

$$n_{\mathrm{eh}} = -\frac{e^2}{2n_0 m_r \omega^2 \epsilon_0}, \tag{2}$$

where e is the elementary charge, n_0 is the unperturbed refractive index for the probe wavelength ($\lambda = 1030$ nm), $1/m_r = 1/m_e + 1/m_h$ is the reduced electron-hole effective mass (m_e and m_h are the electron and hole effective masses, respectively), ω is the circular frequency of the probe light wave, and ϵ_0 is the permittivity of vacuum.

Note that in Eq. (1) we use the *instantaneous* decay time, τ_G, which describes the decay rate at chosen delay time. Under such an approximation, τ_G can be expressed using the reciprocal summation of the recombination time, τ, and the diffusion-grating decay time, τ_D, [28]:

$$\frac{1}{\tau_G} = \frac{1}{\tau} + \frac{1}{\tau_D} = \frac{1}{\tau} + \frac{4\pi^2 D_a}{\Lambda^2}. \tag{3}$$

Equation (3) indicates that one can extract τ and D_a from the linear fit of the dependence $\tau_G^{-1} = f(\Lambda^{-2})$.

All measurements are carried out at room temperature.

III. RESULTS AND DISCUSSION

We begin with the illustration of D_a and τ determination in the "thick" *m*-plane sample. Figure 2(a) shows the LITG transients recorded at various grating periods Λ for two different excitations; the shown transients are rather typical. At both excitations, the LITG decay is visibly faster for smaller Λ values, which indicates the measurable impact of diffusion on grating erasure. τ_G is determined from the exponential fit according to Eq. (1) of the initial part of the LITG transient, within approximately 100 ps after the excitation. We assume that this time span is short enough compared to the carrier lifetime so that the photoexcited carrier density N remains close to N_0. D_a and τ are obtained by fitting Eq. (3) to $1/\tau_G = f(1/\Lambda^2)$, as shown in Fig. 2(b).

In the LITG technique, the carrier density gradient and, thus, the direction of diffusion are parallel to the grating vector. Hence, the anisotropy of the in-plane diffusion can be revealed by rotating a sample, which changes the orientation of the diffusion direction with respect to the crystallographic directions. No changes in D_a values are observed for several random orientations of the *c*-plane sample, while the D_a value in both *m*-plane samples is noticeably anisotropic. Figure 3 shows the D_a (a) and τ (b) values as a function of the angle at two excitations in the "thick" *m*-plane sample; the qualitative picture in the *m*-MQW structure with thin QWs is similar. The 0° (90°) angle corresponds to the grating vector being parallel to the *a* (*c*) direction, as illustrated in Fig. 1(b). We note that pump energy fluences of 90 and 360 μ J/cm^2 result in photoexcited carrier densities of 1.7×10^{19} and 6.8×10^{19} cm^{-3}, respectively. At the lower excitation, D_a changes with the angle from approximately 0.4 cm^2/s along the *c* direction to approximately 2.0 cm^2/s along the *a* direction. The anisotropy of the diffusion coefficient is even clearer at the higher excitation of 360 μJ/cm^2, where D_a increases from approximately 1.3 cm^2/s to approximately 4.5 cm^2/s. We note that the existence of a small peak at 75° is not certain; most likely it represents measurement error. On the other hand, the carrier lifetime does not depend on the sample orientation and drops from approximately 500 ps to approximately 220 ps with increased excitation [Fig. 3(b)]. These results demonstrate that the electron and hole density distribution is isotropic and that the D anisotropy must be related to the transport anisotropy.

Under the given experimental conditions, where electrons and holes are photoexcited in pairs via interband absorption, the carrier transport is of an ambipolar type. The ambipolar diffusion coefficient obtained in the LITG measurements can be expressed via the monopolar diffusion coefficients using the relation [28]

$$D_a = \frac{n + p}{n/D_h + p/D_e}, \tag{4}$$

where $n(p)$ is the electron (hole) density and D_e (D_h) is the monopolar electron (hole) diffusion coefficient. $n \approx p$ because the photoexcited carrier density exceeds the equilibrium electron density by several orders of magnitude, which in our samples is estimated as lower than 10^{17} cm^{-3}. Also, the inequality $D_e \gg D_h$ holds in group-III nitrides due to the electron mobility being much higher than that of the holes. Under the latter approximations, Eq. (4) leads to $D_a \approx 2D_h$, i.e., the ambipolar diffusion is hole governed. In turn, the monopolar diffusion coefficient in a nondegenerate semiconductor is related to the mobility and the effective mass as $D_h = \mu_h k_B T/e = \tau_{\text{scatt}} k_B T/m_h$, where μ_h is the hole mobility, $k_B T$ is the thermal energy, and τ_{scatt} is the hole-momentum scattering time. The differences in

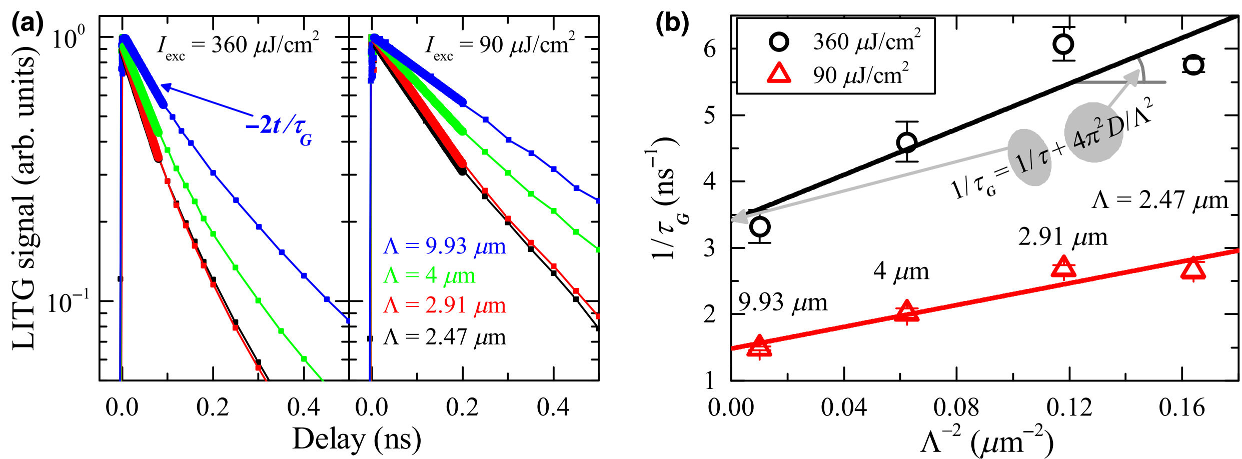

FIG. 2. (a) Normalized LITG transients recorded at four periods Λ (9.93, 4.0, 2.91, and 2.47 μm) and two excitation energy fluences I_{exc} (90 and 360 μJ/cm^2, reflection excluded) in the thick *m*-plane sample. The lines in the initial parts of the transients are exponential fits according to Eq. (1). (b) τ_G^{-1} as a function of Λ^{-2}. The solid lines show the fits according to Eq. (3). The sample is oriented so that carriers diffuse along the *a* axis.

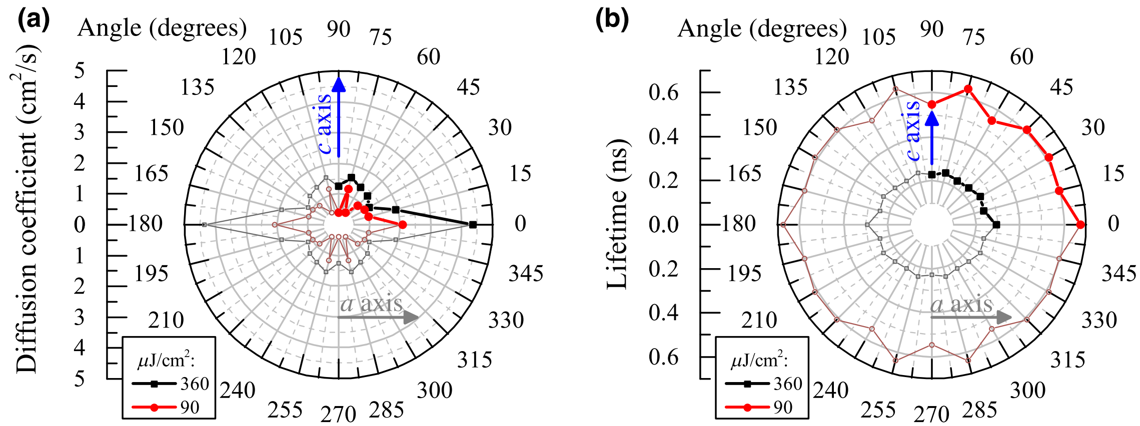

FIG. 3. The measured (a) diffusion coefficient D_a and (b) lifetime τ values as functions of the angle for two excitations of 90 and 360 μJ/cm^2 in the "thick" m-plane sample. The data in the first quadrant represent the measured values, while the points in other three quadrants are obtained by symmetrical reflections of the measured values.

the D_a values can be attributed to the anisotropy of the hole effective mass in the m-plane (In,Ga)N. This assumption is in good agreement with the theoretical works by Park *et al.*, who have calculated a hole effective mass of 0.38 m_0 and 1.91 m_0 (m_0 is electron mass) along the a and c directions, respectively, in the m-plane (In,Ga)N, and by Zhao *et al.*, who have attributed the cause of the valence-band anisotropy to unbalanced biaxial stress [40,41]. Our D_a values are also close to those obtained by Mensi *et al.*, in m-plane QWs (0.4 and 1.9 cm^2/s along and perpendicular to the c direction, respectively), where the diffusion anisotropy has also been attributed to the different hole-mass values [32]. Ščajev *et al.* have also observed the anisotropy of the hole diffusion coefficient in bulk m-plane GaN substrates, but the difference in the D_a values along the perpendicular directions has only been found to be 17% [42] (we note that McLaurin *et al.* have found that the hole mobility in bulk m-plane GaN is isotropic [43]). The much smaller anisotropy of the diffusion coefficient in bulk nonpolar GaN, which lacks biaxial strain, agrees well with the explanation for the anisotropy proposed by Zhao *et al.* [41]. We do not, however, exclude the possibility of some contribution by the compositional disorder to anisotropy of the hole diffusion coefficient. As the compositional fluctuations create internal electric fields and potential barriers in nitrides and these fields are strongest along the c direction in the wurtzite structure, one might expect that such barriers will hinder the motion of carriers in the c direction, which is indeed seen in our results. Also, the use of Einstein's relation between the mobility and the diffusion coefficient might be an approximation in our disordered-alloy system.

Figures 4(a) and 4(b) show the measured diffusion coefficient D_a as a function of the carrier density N in the m-plane and the c-plane samples, respectively. In the thin c-plane MQW structure (Fig. 4(b), blue triangles), $D_a = 0.7$ cm^2/s is approximately constant at low densities and starts to increase with excitation above $N = 4 \times 10^{18}$ cm^{-3}. For the thick c-plane layer as well as the m-plane samples, the diffusion coefficient at low densities behaves differently: it starts from unexpectedly high values (e.g., $D_{\parallel a} = 8$ cm^2/s and $D_{\parallel c} = 2$ cm^2/s at $\approx 10^{18}$ cm^{-3} in the thick m-plane structure), decreases with the excitation until the minimum value at $N \approx 10^{19}$ cm^{-3}, and then begins to increase. An extremely high value of $D_a = 25$ cm^2/s is obtained in the thick c-plane single layer [Fig. 4(b), olive circles]. Let us recall that the low-density D value is $\approx 1 - 2$ cm^2/s in bulk c-plane GaN [42,44]. We note that in the thick m-plane sample, the ratio between the D_a values along the main orthogonal directions remains approximately constant within the entire density range, which supports the proposition that ambipolar diffusion along those directions is governed by hole transport with different effective masses. On the other hand, $D_a(N)$ at high densities does not seem to depend much on the layer thickness.

While the dependence $D_a(N)$ in the thin c-plane MQW sample resembles those observed in other polar (In,Ga)N QW structures [33,45], the kind of behavior seen in the m-plane and thick c-plane samples is untypical. To better understand the processes behind it, we separately analyze the "low-density" region, where $D(N)$ decreases with increasing density, and the "high-density region," where the $D(N)$ dependence is opposite and increases with the excitation.

To discuss the low-density region, we begin with the question of why D_a in the m-plane MQWs and the thick c-plane layer is much higher than that in the c-plane MQW sample. No such dependence has been observed in bulk m-plane or c-plane GaN layers [42,44] or in other

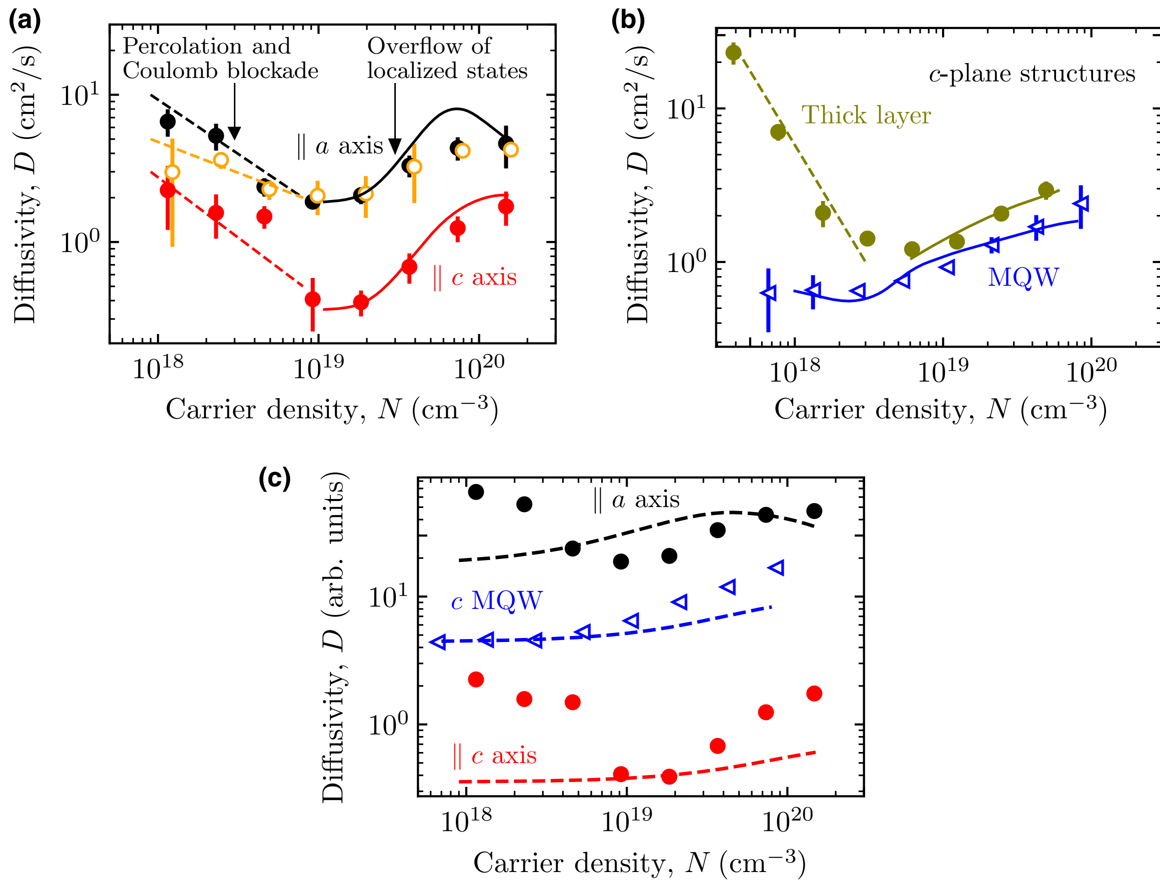

FIG. 4. (a) The measured diffusion coefficient D as a function of the photoexcited carrier density N in the m-plane MQW samples along the $\parallel a$ (black and orange circles for 8-nm and 4-nm wells, respectively) and $\parallel c$ (red circles for 8-nm wells) directions. The dashed lines are guides for the eye to depict the onset of Coulomb blockade along the percolation paths through the localized states. The solid lines show the fits obtained by numerically solving Eqs. (6)–(8). (b) The same $D(N)$ dependences in the thick c-plane layer (olive circles) and the MQW structure (blue triangles). The meaning of the lines is the same as in (a). (c) Fits (dashed lines) of measured $D(N)$ values (symbols), assuming no localization ($N_L = 0$), solving Eqs. (5)–(7). The curves in this figure are arbitrarily shifted with respect to each other for the sake of visibility.

c-plane QW structures [34,45]. These facts suggest that the high diffusivity must be related to the thick layers and compositional disorder.

A possible transport mechanism is due to percolation paths through the disorder-induced localized states, as seen in simulations of MQW LEDs for perpendicular transport. Such simulated percolation paths appear to be at the root of the increased current for a given voltage compared to simulations without disorder [12,46], thereby explaining the diminished turn-on voltage of (In,Ga)N-based LEDs compared to disorderless models. They have also been carefully demonstrated in vertical unipolar transport structures for (In,Ga)N and (Al,Ga)N [47]. Let us remark that bulk or in-plane percolative transport has been observed in bulk semiconductors for a long time, where the disorder is provided by random impurities [48]. In low-dimensional structures, studies of quantum Hall plateaus [49,50] and metal-insulator transitions below the transition threshold [51–53] have also been linked to percolative transport. To then understand the appearance here of the high diffusion coefficients only for thick layers of (In,Ga)N materials, one should recall the universal increase of percolation with system thickness. The role of QW thickness in increasing percolation from such a compositional disorder has recently been discussed by Horton *et al.* [54]. This idea is well supported by our current results: the increase in D_a is the highest in the c-plane layer, which is the thickest in the sample set, and then this value is smaller in the 8-nm-thick m-plane wells and even smaller in the 4-nm m-plane wells [25, 8, and $2-3$ cm^2/s, respectively; see Figs. 4(a) and 4(b)]. Still, these values remain higher than the corresponding D_a value in the even thinner c-plane MQW sample. Therefore, we propose that the high D values at low carrier densities can be explained by efficient hole transport via such percolative paths.

In turn, the decrease of the diffusivity with excitation can occur due to Coulomb blocking in the percolative paths, an effect similar to that in quantum-dot solids, when

occupation of localized states along the percolative paths by carriers hinders the movement of other charge carriers due to the Coulomb interaction between charges [55,56]. A numerical model describing the percolative transport and Coulomb blockade in thick QWs would be challenging, as three-dimensional- (3D) like transport simulations accounting both for compositional disorder and screening of internal electric fields are not yet available. In a simple rule-of-thumb picture, though, one can expect that charging of the localized states occurs at a carrier density N_a such that $a = 1/\sqrt[3]{N_a}$, where a is the size of the localized state. For a typical diameter and separation of 5 nm of the localized states [6,12], the charging is expected to occur at a density of 5×10^{18} cm^{-3}, which is indeed observed in Figs. 4(a) and 4(b). The Coulomb-blockade effect should disappear when the carrier density is such that the Fermi level is above the level of doubly charged localized states—most certainly holes in the present case, as the ambipolar diffusion is dominated by hole transport. This typically occurs at levels of a few tens of millielectronvolts in quantum dots with sizes similar to those of our localized states [55,56], which corresponds to 2×10^{19} cm^{-3} [38], again in the observed range. Another cause for getting above the Coulomb blockade for diffusion is the filling of states above the depth of the localized states, again a few tens of millielectronvolts [12].

In a more quantitative model, the increase of $D(N)$ with density in the high-density region above 10^{19} cm^{-3} can be explained by hole diffusion in a degenerate semiconductor with disorder; however, without having to take into account the carrier diffusion through the localized states. This is reasonable, as there would be many more delocalized carriers than localized ones. Let us first discuss a model without localization: the increase of the hole diffusion constant in a degenerated case cannot be explained by the degenerate hole gas alone, contrary to what has been shown in bulk GaN [44]. To demonstrate this, we model the dependence $D_E(N)$ for holes using the general Einstein relation, which represents the relation between the diffusivity and mobility of charge carriers in degenerate bands of an ordered semiconductor:

$$D_E(N) = \frac{k_B T}{e}\mu A(\eta) = D_0 A(\eta),$$
$$A(\eta) = \frac{F_{1/2}(\eta)}{F_{-1/2}(\eta)}, \quad \eta = \frac{E - E_F}{k_B T}, \tag{5}$$

where D_0 is the low-density diffusion coefficient without localization and the $F_{\pm 1/2}(\eta)$ are the Fermi integrals of the respective order. We stress that D_0 is considered as a fitting parameter in further discussion, as it is not accessible by experiment. In addition, we include the electron-hole scattering, which becomes important and limits the growth of diffusivity at high carrier densities, especially for a small effective mass [57]. We calculate the corresponding diffusion coefficient D_{eh} using the modified Fletcher formula, which models the decrease of diffusion coefficient of carriers due to electron-hole collisions in a classical semiconductor when the electron and hole densities are equal ($n \approx p = N$) [58]:

$$D_{\text{eh}}(N) = 48\pi^{3/2} 2^{-3/2} N^{-1} (\varepsilon\varepsilon_0)^2 e^{-4} \left(\frac{m_e + m_h}{m_e m_h}\right)^{1/2} \times \frac{(k_B T)^{5/2}}{lg[1 + 256 (\varepsilon\varepsilon_0)^2 N^{-2/3} e^{-4} k_B^2 T^2]}, \tag{6}$$

where ϵ is the static relative permittivity of the material and ϵ_0 is the permittivity of vacuum. The overall diffusion constant $D(N)$ is given by a sum of reciprocals:

$$\frac{1}{D(N)} = \frac{1}{D_E(N)} + \frac{1}{D_{\text{eh}}(N)}. \tag{7}$$

The dashed lines in Fig. 4(c) show the calculated dependences; D_0 is varied to adjust the calculated curves to the lowest measured D values. The discrepancy with the measured values is obvious for all cases. For a lower effective mass (along the a axis), Eq. (5) almost recreates the rate of $D(N)$ growth with excitation but noticeably underestimates the density at which the increase should start. For higher effective masses (along the c axis), the diffusion coefficient should increase due to hole-gas degeneracy much less than it does in the experiment. This result suggests that another ingredient should be included, namely structural disorder in (In,Ga)N.

To account for the localization effect in the presence of degeneracy, we adopt the relation proposed by Ščajev *et al.*, which calculates the diffusivity D_{loc} [59]:

$$D_{\text{loc}}(N) = \frac{A(\eta) D_0}{1 + A(\eta)\frac{E_U}{k_B T}\frac{N_L}{N_C}}, \tag{8}$$

where E_U is the Urbach energy, describing the width of the Gaussian distribution of the localization energy, and N_L and N_C are the densities of the localized and free (mobile) carriers ($N = N_L + N_C$). This model is based on the assumption that carriers in the localized states are immobile and that transport occurs only via extended states, which is reasonable in inorganic semiconductors [19]. In addition, carrier localization is considered a very fast process with a time constant of the order of a picosecond. As a result, such a system can be considered in quasiequilibrium in terms of localized-state occupation on the time scale of hundreds of picoseconds.

The solid lines in Figs. 4(a) and 4(b) show the function $D(N)$ calculated from Eqs. (6)–(8) for effective masses of 0.38 m_0 (black) and 1.91 m_0 (red) for the m-plane sample and 1.1 m_0 (blue) for the c-plane MQW sample, using D_{loc} instead of D_E in Eq. (7). In the modeling, D_0

and $E_U \cdot N_L/N_C$ are fitting parameters, the latter being the density function. The presented fits are obtained assuming the same distribution function but different densities of localized states, the latter being lower by an order of magnitude in the *c*-plane sample than in the *m*-plane structure. We believe that this difference in N_L values reflects the different dimensionality of density of states in these samples: the 3D density of states in the thick *m*-plane sample provides a higher amount of states if compared to the two-dimensional case in the thin *c*-plane MQW sample. The fits obtained using Eq. (8) follow the diffusion coefficient in the high-density region much more closely, proving that carrier delocalization due to the overflow of localized states plays an important role in diffusivity even at such high densities.

Finally, we discuss the relevance of the presented results to the understanding and optimization of nitride-based LEDs. Experiments coupled with 3D simulations have corroborated that the polarization barriers present in long-wavelength *c*-plane LEDs limit vertical transport of holes and contribute to the large excess voltage of green LEDs relative to their blue counterparts, resulting in a power-conversion efficiency loss, and are a major contributor to the so-called "green gap" [60]. For long-wavelength *c*-plane LEDs, it has been demonstrated that these limits to vertical injection can be overcome through the use of inverted hexagonal *V* defects, where hole injection occurs in parallel into all the QWs of the active LED layer via the *V*-defect semipolar sidewall [61–63]. LEDs containing engineered *V* defects currently represent the most promising path to achieving high wall plug efficiency (WPE) long-wavelength devices. However, despite the demonstration of a high WPE at low current using *V* defects [62,63], the LEDs still exhibit significant current droop, indicating that it is now the in-plane hole transport that hampers complete volumetric injection of multiple QWs. Mitigation of the current droop using *V* defects and optimized hole-transport structures represents an important opportunity for the advancement of nitride LEDs. Knowledge of hole diffusion in (In,Ga)N alloys and mitigating structures will enable rational heterostructure design through both experimental and 3D simulation methods, such as those carried out by Li *et al.* [64].

For such mitigation studies, in addition to experimental *V*-defect engineering, the critical in-plane hole diffusion parameters are required as inputs for accurate device simulation. Simulations of LEDs with (In,Ga)N alloy active layers require the incorporation of alloy-disorder effects. Simple one-dimensional simulation tools, therefore not including in-plane compositional fluctuations, lead to excessive onset voltages compared to experiments. Recent 3D simulations including disorder show much improved agreement with experiment and therefore provide an extremely useful tool to further improve LED performance [12,46,60]. However, these modeling tools require input parameters that are not straightforward to measure by usual techniques. This is particularly true for carrier transport parameters, which require doped materials, whereas the active layers of LEDs are undoped, introducing some variance of measured parameters with those of LED materials, and which, in addition, are typically taken as constant with the carrier density in simulations. Therefore, the presented results obtained by the LITG technique provide valuable information regarding the variation of the diffusion coefficient, and hence the mobility, with the carrier density in undoped material. This situation is commonly encountered when computing I-V characteristics where carrier densities vary by two orders of magnitude in the range of interest. By separating lateral from vertical transport effects, LITG measurements can be used to understand and optimize nitride LEDs.

IV. CONCLUSIONS

We apply the light-induced transient-grating technique to study the hole diffusion in unintentionally doped *c*-plane and *m*-plane (In,Ga)N QW structures. The diffusion coefficient in *m*-plane QWs is anisotropic, up to 5 times higher along the *a* crystallographic axis if compared to that along the *c* axis. This difference arises due to anisotropy of the hole effective mass in the topmost valence band. While the diffusion coefficient strongly depends on the carrier density, this dependence differs in thick and thin structures. We suggest that the high diffusivity at low carrier densities in thick structures can be explained by efficient hole transport via percolative paths related to compositional disorder and that a sufficient thickness of layers leads to increased percolative 3D-like transport, i.e., large diffusion coefficients. In turn, the drop of the diffusivity with the carrier density in the range below 10^{19} cm^{-3} can tentatively be attributed to Coulomb blocking of these percolative paths. Alternatively, at carrier densities above 10^{19} cm^{-3}, the growth of the diffusivity with the carrier density could be explained by the cumulative effect of hole-gas degeneracy and overflow of localized states. The obtained understanding of the hole diffusion dependence on carrier density and QW thickness can be useful for LED modeling tools that require transport parameters of undoped (In,Ga)N.

ACKNOWLEDGMENTS

The research at Vilnius University was supported by the Lithuanian Research Council, under Contract No. S-MIP-17-75. The research at the University of California, Santa Barbara was supported by the Solid State Lighting and Energy Electronics Center (SSLEEC), U.S. Department of Energy, under Award No. DE-EE0008204, the National Science Foundation, under Grant No. DMS-1839077, and by grants from the Simons Foundation (Grants No. 601952 to J.S. and No. 601954 to C.W.).

[1] C. A. Hurni, A. David, M. J. Cich, R. I. Aldaz, B. Ellis, K. Huang, A. Tyagi, R. A. Delille, M. D. Craven, F. M. Steranka, and M. R. Krames, Bulk GaN flip-chip violet light-emitting diodes with optimized efficiency for high-power operation, Appl. Phys. Lett. **106**, 031101 (2015).

[2] C. Weisbuch, M. Piccardo, L. Martinelli, J. Iveland, J. Peretti, and J. S. Speck, The efficiency challenge of nitride light-emitting diodes for lighting, Phys. Status Solidi (A) **212**, 899 (2015).

[3] S. J. Rosner, E. C. Carr, M. J. Ludowise, G. Girolami, and H. I. Erikson, Correlation of cathodoluminescence inhomogeneity with microstructural defects in epitaxial GaN grown by metalorganic chemical-vapor deposition, Appl. Phys. Lett. **70**, 420 (1997).

[4] W. Liu, J.-F. Carlin, N. Grandjean, B. Deveaud, and G. Jacopin, Exciton dynamics at a single dislocation in GaN probed by picosecond time-resolved cathodoluminescence, Appl. Phys. Lett. **109**, 042101 (2016).

[5] S. Chichibu, T. Azuhata, T. Sota, and S. Nakamura, Spontaneous emission of localized excitons in InGaN single and multiquantum well structures, Appl. Phys. Lett. **69**, 4188 (1996).

[6] W. Hahn, J.-M. Lentali, P. Polovodov, N. Young, S. Nakamura, J. S. Speck, C. Weisbuch, M. Filoche, Y.-R. Wu, M. Piccardo, F. Maroun, L. Martinelli, Y. Lassailly, and J. Peretti, Evidence of nanoscale Anderson localization induced by intrinsic compositional disorder in InGaN/GaN quantum wells by scanning tunneling luminescence spectroscopy, Phys. Rev. B **98**, 045305 (2018).

[7] C. Humphreys, J. Griffiths, F. Tang, F. Oehler, S. Findlay, C. Zheng, J. Etheridge, T. Martin, P. Bagot, M. Moody, D. Sutherland, P. Dawson, S. Schulz, S. Zhang, W. Fu, T. Zhu, M. Kappers, and R. Oliver, The atomic structure of polar and non-polar InGaN quantum wells and the green gap problem, Ultramicroscopy **176**, 93 (2017).

[8] S. Schulz, M. A. Caro, C. Coughlan, and E. P. O'Reilly, Atomistic analysis of the impact of alloy and well-width fluctuations on the electronic and optical properties of InGaN/GaN quantum wells, Phys. Rev. B **91**, 035439 (2015).

[9] S. Schulz, D. P. Tanner, E. P. O'Reilly, M. A. Caro, T. L. Martin, P. A. J. Bagot, M. P. Moody, F. Tang, J. T. Griffiths, F. Oehler, M. J. Kappers, R. A. Oliver, C. J. Humphreys, D. Sutherland, M. J. Davies, and P. Dawson, Structural, electronic, and optical properties of *m*-plane InGaN/GaN quantum wells: Insights from experiment and atomistic theory, Phys. Rev. B **92**, 235419 (2015).

[10] J. T. Griffiths, S. Schulz, P. Dawson, M. A. Caro, M. J. Davies, C. J. Humphreys, D. S. P. Tanner, R. A. Oliver, E. P. O'Reilly, F. Tang, M. J. Kappers, F. Oehler, and D. Sutherland, Theoretical and experimental analysis of the photoluminescence and photoluminescence excitation spectroscopy spectra of *m*-plane InGaN/GaN quantum wells, Appl. Phys. Lett. **109**, 223102 (2016).

[11] P. Dawson, S. Schulz, R. A. Oliver, M. J. Kappers, and C. J. Humphreys, The nature of carrier localisation in polar and nonpolar InGaN/GaN quantum wells, J. Appl. Phys. **119**, 181505 (2016).

[12] C. K. Li, M. Piccardo, Y. R. Wu, J. S. Speck, B. Bonef, R. M. Farrell, M. Filoche, L. Martinelli, J. Peretti, and C. Weisbuch, Localization landscape theory of disorder in semiconductors. II. Urbach tails of disordered quantum well layers, Phys. Rev. B **95**, 144206 (2017).

[13] S. Y. Karpov, Carrier localization in InGaN by composition fluctuations: Implication to the "green gap", Photonics Res. **5**, A7 (2017).

[14] D. S. P. Tanner, P. Dawson, M. J. Kappers, R. A. Oliver, and S. Schulz, Polar InGaN/GaN Quantum Wells: Revisiting the Impact of Carrier Localization on the Green Gap Problem, Phys. Rev. Appl. **13**, 044068 (2020).

[15] M. Shahmohammadi, W. Liu, G. Rossbach, L. Lahourcade, A. Dussaigne, C. Bougerol, R. Butté, N. Grandjean, B. Deveaud, and G. Jacopin, Enhancement of Auger recombination induced by carrier localization in InGaN/GaN quantum wells, Phys. Rev. B **95**, 125314 (2017).

[16] C. M. Jones, C. H. Teng, Q. Yan, P. C. Ku, and E. Kioupakis, Impact of carrier localization on recombination in InGaN quantum wells and the efficiency of nitride light-emitting diodes: Insights from theory and numerical simulations, Appl. Phys. Lett. **111**, 113501 (2017).

[17] R. Aleksiejūnas, K. K. Gelžinytė, S. Nargelas, K. Jarašiūnas, M. Vengris, E. A. Armour, D. P. Byrnes, R. A. Arif, S. M. Lee, and G. D. Papasouliotis, Diffusion-driven and excitation-dependent recombination rate in blue InGaN/GaN quantum well structures, Appl. Phys. Lett. **104**, 022114 (2014).

[18] Y.-H. Cho, G. H. Gainer, A. J. Fischer, J. J. Song, S. Keller, U. K. Mishra, and S. P. DenBaars, "S-shaped" temperature-dependent emission shift and carrier dynamics in InGaN/GaN multiple quantum wells, Appl. Phys. Lett. **73**, 1370 (1998).

[19] J. Bisquert, Interpretation of electron diffusion coefficient in organic and inorganic semiconductors with broad distributions of states, Phys. Chem. Chem. Phys. **10**, 3175 (2008).

[20] M. Ansari-Rad, J. A. Anta, and J. Bisquert, Interpretation of diffusion and recombination in nanostructured and energy-disordered materials by stochastic quasiequilibrium simulation, J. Phys. Chem. C **117**, 16275 (2013).

[21] T. H. Gfroerer, Y. Zhang, and M. W. Wanlass, An extended defect as a sensor for free carrier diffusion in a semiconductor, Appl. Phys. Lett. **102**, 012114 (2013).

[22] F. Chen, Y. Zhang, T. H. Gfroerer, A. N. Finger, and M. W. Wanlass, Spatial resolution versus data acquisition efficiency in mapping an inhomogeneous system with species diffusion, Sci. Rep. **5**, 10542 (2015).

[23] R. Richert, L. Pautmeier, and H. Bässler, Diffusion and Drift of Charge Carriers in a Random Potential: Deviation from Einstein's Law, Phys. Rev. Lett. **63**, 547 (1989).

[24] Y. Roichman and N. Tessler, Generalized Einstein relation for disordered semiconductors—Implications for device performance, Appl. Phys. Lett. **80**, 1948 (2002).

[25] R. Aleksiejūnas, M. Sūdžius, T. Malinauskas, J. Vaitkus, K. Jarašiūnas, and S. Sakai, Determination of free carrier bipolar diffusion coefficient and surface recombination velocity of undoped GaN epilayers, Appl. Phys. Lett. **83**, 1157 (2003).

[26] A. Vertikov, I. Ozden, and A. V. Nurmikko, Investigation of excess carrier diffusion in nitride semiconductors with near-field optical microscopy, Appl. Phys. Lett. **74**, 850 (1999).

[27] J. Danhof, U. T. Schwarz, A. Kaneta, and Y. Kawakami, Time-of-flight measurements of charge carrier diffusion in $In_xGa_{1-x}N$/GaN quantum wells, Phys. Rev. B **84**, 035324 (2011).

[28] H. J. Eichler, P. Gunter, and D. W. Pohl, *Laser-Induced Dynamic Gratings* (Springer-Verlag, New York, 1986).

[29] A. Vertikov, I. Ozden, and A. V. Nurmikko, Diffusion and relaxation of excess carriers in InGaN quantum wells in localized versus extended states, J. Appl. Phys. **86**, 4697 (1999).

[30] A. Kaneta, T. Hashimoto, K. Nishimura, M. Funato, and Y. Kawakami, Visualization of the local carrier dynamics in an InGaN quantum well using dual-probe scanning near-field optical microscopy, Appl. Phys. Express **3**, 102102 (2010).

[31] H.-M. Solowan, J. Danhof, and U. T. Schwarz, Direct observation of charge carrier diffusion and localization in an InGaN multi quantum well, Jpn. J. Appl. Phys. **52**, 08JK07 (2013).

[32] M. Mensi, R. Ivanov, T. K. Uždavinys, K. M. Kelchner, S. Nakamura, S. P. DenBaars, J. S. Speck, and S. Marcinkevičius, Direct measurement of nanoscale lateral carrier diffusion: Toward scanning diffusion microscopy, Acs Photonics **5**, 528 (2017).

[33] R. Aleksiejūnas, P. Ščajev, S. Nargelas, T. Malinauskas, A. Kadys, and K. Jarašiūnas, Impact of diffusivity to carrier recombination rate in nitride semiconductors: From bulk GaN to (In, Ga) N quantum wells, Jpn. J. Appl. Phys. **52**, 08JK01 (2013).

[34] K. Nomeika, R. Aleksiejūnas, S. Miasojedovas, R. Tomašiūnas, K. Jarašiūnas, I. Pietzonka, M. Strassburg, and H. J. Lugauer, Impact of carrier localization and diffusion on photoluminescence in highly excited cyan and green InGaN LED structures, J. Lumin. **188**, 301 (2017).

[35] Z. Ye, H. Nguyen, S.-W. Feng, H.-C. Wang, and H.-L. Chou, Carrier dynamics in InGaN/GaN on the basis of different In concentrations, Appl. Sci. **9**, 2279 (2019).

[36] K. Jarašiūnas, R. Aleksiejūnas, T. Malinauskas, V. Gudelis, T. Tamulevičius, S. Tamulevičius, A. Guobienė, A. Usikov, V. Dmitriev, and H. J. Gerritsen, Implementation of diffractive optical element in four-wave mixing scheme for *ex situ* characterization of hydride vapor phase epitaxy-grown GaN layers, Rev. Sci. Instrum. **78**, 033901 (2007).

[37] T. Malinauskas, S. Nargelas, R. Aleksiejūnas, and K. Jarašiūnas, Heterodyne detection scheme for light-induced transient grating experiment, Opt. Commun. **281**, 6061 (2008).

[38] M. Feneberg, S. Osterburg, K. Lange, C. Lidig, B. Garke, R. Goldhahn, E. Richter, C. Netzel, M. D. Neumann, N. Esser, S. Fritze, H. Witte, J. Bläsing, A. Dadgar, and A. Krost, Band gap renormalization and Burstein-Moss effect in silicon- and germanium-doped wurtzite GaN up to 10^{20} cm^{-3}, Phys. Rev. B **90**, 075203 (2014).

[39] C. Shank, R. Fork, R. Yen, J. Shah, B. Greene, A. Gossard, and C. Weisbuch, Picosecond dynamics of hot carrier relaxation in highly excited multi-quantum well structures, Solid State Commun. **47**, 981 (1983).

[40] S. H. Park, D. Ahn, and S. L. Chuang, Electronic and optical properties of *a*- and *c*-plane wurtzite InGaN-GaN quantum wells, IEEE J. Quantum Electron. **43**, 1175 (2007).

[41] Y. Zhao, R. M. Farrell, Y.-R. Wu, and J. S. Speck, Valence band states and polarized optical emission from nonpolar and semipolar III-nitride quantum well optoelectronic devices, Jpn J. Appl. Phys. **53**, 100206 (2014).

[42] P. Ščajev, K. Jarašiūnas, Ü. Özgür, H. Morkoç, J. Leach, and T. Paskova, Anisotropy of free-carrier absorption and diffusivity in *c*-plane GaN, Appl. Phys. Lett. **100**, 022112 (2012).

[43] M. McLaurin and J. S. Speck, *p*-type conduction in stacking-fault-free *m*-plane GaN, Phys. Status Solidi (RRL)—Rapid Res. Lett. **1**, 110 (2007).

[44] T. Malinauskas, K. Jarašiūnas, M. Heuken, F. Scholz, and P. Brückner, Diffusion and recombination of degenerate carrier plasma in GaN, Phys. Status Solidi (C) **6**, S743 (2009).

[45] R. Aleksiejūnas, K. Nomeika, S. Miasojedovas, S. Nargelas, T. Malinauskas, K. Jarašiūnas, Ö Tuna, and M. Heuken, Carrier dynamics in blue and green emitting InGaN MQWs, Phys. Status Solidi (B) **252**, 977 (2015).

[46] T.-J. Yang, R. Shivaraman, J. S. Speck, and Y.-R. Wu, The influence of random indium alloy fluctuations in indium gallium nitride quantum wells on the device behavior, J. Appl. Phys. **116**, 113104 (2014).

[47] D. A. Browne, M. N. Fireman, B. Mazumder, L. Y. Kuritzky, Y.-R. Wu, and J. S. Speck, Vertical transport through AlGaN barriers in heterostructures grown by ammonia molecular beam epitaxy and metalorganic chemical vapor deposition, Semicond. Sci. Technol. **32**, 025010 (2017).

[48] B. I. Shklovskii and A. L. Efros, *Electronic Properties of Doped Semiconductors*, Springer Series in Solid-State Sciences (Springer-Verlag, Berlin, 1984).

[49] R. F. Kazarinov and S. Luryi, Quantum percolation and quantization of Hall resistance in two-dimensional electron gas, Phys. Rev. B **25**, 7626 (1982).

[50] D.-H. Lee, Z. Wang, and S. Kivelson, Quantum Percolation and Plateau Transitions in the Quantum Hall Effect, Phys. Rev. Lett. **70**, 4130 (1993).

[51] L. A. Tracy, E. H. Hwang, K. Eng, G. A. Ten Eyck, E. P. Nordberg, K. Childs, M. S. Carroll, M. P. Lilly, and S. Das Sarma, Observation of percolation-induced two-dimensional metal-insulator transition in a Si MOSFET, Phys. Rev. B **79**, 235307 (2009).

[52] J.-S. Kim, A. M. Tyryshkin, and S. A. Lyon, Annealing shallow Si/SiO2 interface traps in electron-beam irradiated high-mobility metal-oxide-silicon transistors, Appl. Phys. Lett. **110**, 123505 (2017).

[53] A. Sammak, D. Sabbagh, N. W. Hendrickx, M. Lodari, B. P. Wuetz, A. Tosato, L. Yeoh, M. Bollani, M. Virgilio, M. A. Schubert, P. Zaumseil, G. Capellini, M. Veldhorst, and G. Scappucci, Shallow and undoped germanium quantum wells: A playground for spin and hybrid quantum technology, Adv. Funct. Mater. **29**, 1807613 (2019).

[54] M. K. Horton and M. A. Moram, Alloy composition fluctuations and percolation in semiconductor alloy quantum wells, Appl. Phys. Lett. **110**, 162103 (2017).

[55] H. E. Romero and M. Drndic, Coulomb Blockade and Hopping Conduction in PbSe Quantum Dots, Phys. Rev. Lett. **95**, 156801 (2005).

[56] R. E. Chandler, A. J. Houtepen, J. Nelson, and D. Vanmaekelbergh, Electron transport in quantum dot solids: Monte Carlo simulations of the effects of shell filling, Coulomb repulsions, and site disorder, Phys. Rev. B **75**, 085325 (2007).

[57] N. H. Fletcher, The high current limit for semiconductor junction devices, Proc. IRE **45**, 862 (1957).

[58] A. H. Hill, K. E. Smyser, C. L. Kennedy, E. S. Massaro, and E. M. Grumstrup, Screened charge carrier transport in methylammonium lead iodide perovskite thin films, J. Phys. Chem. Lett. **8**, 948 (2017).

[59] P. Ščajev, C. Qin, R. Aleksiejūnas, P. Baronas, S. Miasojedovas, T. Fujihara, T. Matsushima, C. Adachi, and S. Juršėnas, Diffusion enhancement in highly excited $MAPbI_3$ perovskite layers with additives, J. Phys. Chem. Lett. **9**, 3167 (2018).

[60] C. Lynsky, A. I. Alhassan, G. Lheureux, B. Bonef, S. P. DenBaars, S. Nakamura, Y.-R. Wu, C. Weisbuch, and J. S. Speck, Barriers to carrier transport in multiple quantum well nitride-based *c*-plane green light emitting diodes, Phys. Rev. Mater. **4**, 054604 (2020).

[61] Z. Quan, L. Wang, C. Zheng, J. Liu, and F. Jiang, Roles of *V*-shaped pits on the improvement of quantum efficiency in InGaN/GaN multiple quantum well light-emitting diodes, J. Appl. Phys. **116**, 183107 (2014).

[62] F. Jiang, J. Zhang, L. Xu, J. Ding, G. Wang, X. Wu, X. Wang, C. Mo, Z. Quan, X. Guo, C. Zheng, S. Pan, and J. Liu, Efficient InGaN-based yellow-light-emitting diodes, Photonics Res. **7**, 144 (2019).

[63] S. Zhang, J. Zhang, J. Gao, X. Wang, C. Zheng, M. Zhang, X. Wu, L. Xu, J. Ding, Z. Quan, *et al.*, Efficient emission of InGaN-based light-emitting diodes: Toward orange and red, Photonics Res. **8**, 1671 (2020).

[64] C.-K. Li, C.-K. Wu, C.-C. Hsu, L.-S. Lu, H. Li, T.-C. Lu, and Y.-R. Wu, 3D numerical modeling of the carrier transport and radiative efficiency for InGaN/GaN light emitting diodes with V-shaped pits, AIP Adv. **6**, 055208 (2016).